Special Issue Article

Visualization of the Secondary Phase in LFP Ingots with Advanced Mapping Techniques[†]

Yulong Liu,[1] Mohammad Norouzi Banis,[1] Wei Xiao,[1,2] Ruying Li,[1] Zhiqiang Wang,[2] Keegan R. Adair,[1] Steeve Rousselot,[3] Pierre Sauriol,[4] Mickaël Dollé,[3] Guoxian Liang,[5] Tsun-Kong Sham,[2] Xueliang Sun[1,]*

[1]Department of Mechanical and Materials Engineering, Western University, London, Ontario, Canada N6A 5B9

[2]Department of Chemistry, Western University, London, Ontario, Canada N6A 5B7 [3]Department of Chemistry, University of Montreal, Montréal, Quebec, Canada, H3C 3J7[4]Department of Chemical Engineering, École Polytechnique de Montréal, Montréal, Quebec, Canada, H3T 1J4

[5]Johnson Matthey Battery Materials Ltd., 280 Ave. Liberté, Candiac, Quebec, Canada, J5R 6X1

*Corresponding author email: xsun@eng.uwo.ca

ABSTRACT

LiFePO$_4$ has been widely used as a cathode material in lithium ion batteries. However, some impurity phases existing in LiFePO$_4$ have a significant influence on its electrochemical performance. Therefore, detection of the impurity phases is necessary for the manufacturer in order to improve the quality of LiFePO$_4$. In particular, visualization of the impurity and secondary phase distributions immersed in the bulk LiFePO$_4$ crystal can help to understand the origin of the impurity and secondary phases, providing clear guidance towards the synthesis of high purity LiFePO$_4$. The results show that with the combination of Raman and EDS, we are capable of identifying the low melting lithium phosphate phase in LFP ingot. Through Micro XRF mapping, more detailed information about the LFP materials after carbon coating are observed. The secondary phases are easily defined due to the high sensitivity of this technology. This article is protected by copyright. All rights reserved

INTRODUCTION

As one of the popular cathode materials for lithium ion batteries, LiFePO$_4$ (LFP) has received increasing attention since its first use in 1997.[1] Application of LFP electrodes in electric transportation has achieved great success in recent years due to its safety and stable cycle performance.[2–4] However, LFP still suffers from the presence of impurity/secondary phases, which have a dramatic influence on the consistency of the LFP materials. Synthesis of high purity LFP materials requires a deep understanding about the origin of the secondary phases in LFP.[2,5–7] Usually, the impurity and secondary phases in LFP are detected and analyzed by the X-ray diffraction (XRD) technique. XRD enables the identification of impurity/secondary phases in LFP powders, but it would be more informative to visualize the distribution of the secondary phases with advanced techniques such as phase mapping. In addition, the sensitivity of XRD is limited due to the low amount of impurity phases in LFP bulk samples. Better identification on the distribution of phases in LFP materials can greatly help in understanding the mechanism of secondary phase formation. More importantly, the obtained information provides guidance to manufacturers in removing the secondary phases or reducing them during LFP synthesis.

LFP has an intrinsically low electronic conductivity, therefore, carbon coating is necessary to increase its conductivity.[8,9] Due to the strong reducing atmosphere at high temperatures during carbon coating processes, there is a possibility of forming secondary phases in LFP materials.[5,7] The phase separation from the LFP crystals is detrimental for electrochemical performance and should be prevented. For this reason it is necessary to identify the secondary phases and where they reside.[5] Thus, it is critical to obtain solid evidence towards the presence and distribution of the phases in LFP after carbon coating. LFP ingot, which has a flat surface after polishing, could serve as a desired model sample for the observation of phase changes during carbon coating.[10] The phase distribution will be visualized using mapping techniques, which can provide a better understanding of the carbon coating process on LFP materials.

In this paper, we will take advantage of mapping techniques including energy dispersive spectroscopy (EDS) mapping, Raman mapping, and Micro X-ray fluorescence (XRF) mapping to evaluate the distribution impurity/secondary phases in LFP materials. In the present work, by using advanced EDS, Raman, and XRF mapping, we successfully identify the low melting phase in LiFePO$_4$ ingot and gather chemical and physical information of the secondary phases formed

in LiFePO$_4$ materials during the carbon coating process. The obtained information will be beneficial for the synthesis of LiFePO$_4$ and C-LiFePO4 materials with less impurities.

EXPERIMENTAL

Carbon Coating on LFP

The LFP ingot sample was provided by Phostech Lithium Inc. (Now, Johnson Matthey, Montreal, Canada).[11] The ingot sample was chosen due to a two-fold reason: first, the typical behaviors of the ingot samples are applicable for ordinary LFP materials; and second, this ingot offers a flat, smooth and polished surface that is ideal for the observation and investigation of the surface chemistry changes during carbon coating, for both the bulk olivine phase and secondary phases. The experimental details of the melt-casting process of LFP ingot materials can be found in previous works.[12,13]

Here, we used the LFP ingot as a raw material and cut it into small sized pieces first. In order to obtain a flat surface on the ingot, we polished the sample using sandpaper (London, 3M Canada) from coarse (Grit 120) to fine grades (Grit 1500). A clean LFP ingot sample is obtained after three 15-minute stints of ultrasonic cleaning in ethanol.

To coat the ingot samples with carbon, a spray-pyrolysis method was adopted. In the experiment, ethanol was used as the carbon precursor and high purity Ar gas was used as carrier and protecting gas. Briefly, the ingot sample with the flat surface up was put in a quartz tube in Al$_2$O$_3$ crucibles with tight seal using vacuum grease and Ar was introduced into the quartz tube for 20 min to eliminate the air. Next, the furnace was heated at a heating rate of 5 ℃/min, and the carbon-coating process was performed at temperatures ranging from 800–900 ℃ for 20 min. After the carbon coating process at high temperatures, the coated sample was cooled to 25 ℃ naturally within the furnace while still under Ar protection.

X-ray Diffraction

Crystal structure and phase composition of LFP samples were collected using X-ray diffraction with θ/2θ mode (D8 Advance, Bruker) in the range of 10–90°, and the step rate was 0.01° per seconds.

Energy Dispersive Spectroscopy Mapping

The LFP or carbon coated LFP (Au coated as conductive agent) were transferred to a Hitachi 4 800 SEM equipped with an energy dispersive spectroscopy (EDS) detector. The accelerating voltage of EDS mapping was 20 kV.

Raman Mapping

The Raman spectra were obtained on a HORIBA Scientific LabRAM with a laser ($\lambda = 532.3$ nm) as the excitation source. Raman spectroscopy maps were collected in autofocus mode with a spatial resolution of ~2 μm.

Micro X-ray Fluorescence Mapping

The samples were mounted on a carbon tape and transferred into the chamber. The X-ray fluorescence mapping (XRF) was carried out in the VESPERS (very sensitive elemental and structural probe employing radiation from a synchrotron) beamline at Canadian Light Sources, University of Saskatoon, Saskatoon, Canada. The characteristic X-ray fluorescence of the samples was detected by a Silicon drift detector at a distance of 50 mm, and the detector was perpendicular to the direction of the incoming X-ray beam. Ion chambers filled with N_2 were used to monitor the flux of X-ray beam. To obtain micro-focusing of the incident beams, KB mirrors were installed. The Fe K edge signals were captured by rastering the samples in steps of 10 μm in length.

RESULTS AND DISCUSSION

Raman Mapping

The LFP ($LiFePO_4$) ingots were prepared and then polished with sand paper to get a flat surface for observations. LFP ingot contains some low melting lithium phosphate phases after synthesis, as shown in Figure 1a. However, the crystal structure information of the low melting phase is hard to define since the concentration is too small or it is in amorphous state. From the phase diagram of Li_2O-P_2O_5, we know that there are several types of phosphates that exist at 25 °C e.g., $LiPO_3$, $Li_4P_2O_7$, Li_3PO_4, and eutectic phases of $LiPO_3$, and $Li_4P_2O_7$. Each of these phosphates have special characteristic finger print peaks in Raman because of their unique and

characteristic P-O bond vibrations (Figure S1). Therefore, Raman is a powerful technique to identify the crystal structure of the low melting phosphate phase in LFP. As shown in the optical image of Figure 2b, it can be seen that there are two different regions with different contrast. Raman point spectra are recorded at both regions. The brighter region (point 1) shows a strong peak at v_1 (953 cm^{-1}), related to the symmetric stretching bond of P-O, which is characteristic peak of LFP material (as the standard LFP spectroscopy shows). Two extra strong peaks of asymmetric bend bond (v_2, 731 cm^{-1}) and asymmetric stretch bond (v_3, 1 046 cm^{-1}) are observed in the lower contrast region. Since these two peaks are the characteristic peaks for the $Li_4P_2O_7$ phase (see the standard spectra in Figure 2a), therefore, the lower contrast region of the low melting phase can be assigned to the $Li_4P_2O_7$ phase.

Raman mapping can identify the phase distribution on solid materials. The mapping function is realized by recording the spectra of the materials point by point. The result of the Raman mapping on the LFP ingot is presented in Figures 3a–c, coupled with corresponding EDS mapping Figure 3d recorded at the same region. It is observed in the SEM-EDS mapping that there is a strip region where the P is rich and Fe is deficient. In the Raman mapping, however, it can be clearly seen from Figure 3b that the phase in the strip region is $Li_4P_2O_7$ (v_3 signal of $Li_4P_2O_7$ is strong). A closer look at the optical image of Figure 2b reveals that the region of darker colour is overlapped with the region where the v_3 signal shows a stronger intensity in the mapping result. The rest of the brighter region is assigned to the LFP phase with a strong v_1 signal, exhibiting a very uniform chemical distribution (Figure 3c). Figure 3a is a combination signal of v_1 and v_3 bonds. As the intensity of the signals are uniform in the observed region, it is suggested that only $Li_4P_2O_7$ and LFP phases are detected.

Micro X-ray Fluorescence Mapping

Carbon coating is one of the most effective methods to improve the conductivity of LFP materials and limit the particle growth during thermal treatment. However, there is the possibility of phase changes on the surface of LFP after carbon coating due to the strong reducing atmosphere at high temperatures (Figure 1b). We had reported a new chemical surface phase, $Fe_2P_2O_7$, which was produced after the loss of Li_2O from LFP, exhibiting a different structure on the LFP ingot surface.[11] In our recent study, another iron-rich conductive phase, Fe_2P, was

observed on the LFP surface accompanied by a surface change of the LFP ingot when increasing the carbon coating temperature.[14] Since the two new phases have different Fe content compared with LFP, it is very interesting to know the Fe element distribution on LFP surfaces after carbon coating. Herein, we conducted XRF (X-ray Fluorescence) mappings of Fe K-edge for different LiFePO$_4$ ingot materials at the VESPERS (Very Sensitive Elemental and Structural Probe Employing Radiation) beamline of Canadian Light Sources, which was capable of delivering a micro-focused hard X-ray beam to solid materials and collecting X-Ray fluorescence (XRF) for elemental distribution. The VESPERS beamline can harness the spectral energy range of 6–30 keV with the spot size of 4 μm ×4 μm.

Figure 4 shows the corresponding XRF and EDS mappings of LFP ingot samples with carbon coating at different temperatures (4a 800, 4b 850, 4c 875, and 4d 900 °C). The XRF mapping with different colours correspond to different normalized Fe K-edge XAS intensities, which can clearly demonstrate the evolution of impurities after annealing at different temperatures. For the LFP ingot sample treated at 800 °C, a large amount of Fe-rich phases can be observed in Figure 4a. Comparing the XRF mapping with the SEM image and EDS mapping, some interesting information is revealed. The XRF mapping is usually conducted at a specific energy, which enables its high sensitivity. As marked by the dashed lines in Figures 4a and e, the shape of the Fe rich region is similar to the shape of the island shown in the SEM images.[11] The impurity phase is assigned to the Fe$_2$P$_2$O$_7$ phase as outlined in our previous reports, which means the secondary phase distribution through the XRF mapping is well-resolved.[11] In contrast, it is hard to separate the Fe$_2$P$_2$O$_7$ phase in the EDS Fe mapping as the change in Fe amount is small (Figure 3e). When increasing the carbon coating temperature to 850 °C, these Fe enriched phases tend to reduce as shown in the XRF mapping of Figure 4b, which is consistent with SEM /EDS mapping in Figure 2f, where a flat surface and uniform elemental distributions are observed. The results are also consistent with the XRD results in Figure S2, indicating that XRF mapping is very sensitive to the phase change in LFP ingot.

As identified in SEM and EDS mapping (Figures 4f and g), some ball-shaped islands tend to emerge upon increasing the temperature of the carbon coating to 875 °C, and the corresponding structures are attributed to Fe-rich phases.[14] In the case of the LFP sample coated at 900 °C (Figure 4d), the Fe-rich phases (regions) grow larger compared with that of the LFP sample

coated at 875 °C (Figure 4c). The results from XRF mappings further confirm the formation of the Fe-rich phase, which may be related to the appearance of the Fe_2P phase based on our recent study, which is in agreement with the XRD result in Figure S3.[14] More interestingly, it is seen that the shape of the Fe rich region in Figure 4d is similar to the shape of the Fe rich region in Figure 4h. Therefore, XRF mapping can provide very strong evidence to support the formation of ball-shaped Fe rich phases on LFP surfaces after carbon coating at high temperatures.

CONCLUSION

We demonstrated the visualization of the impurity/secondary phases in LFP using EDS, Raman, and micro XRF mapping techniques. Application of these advanced mapping techniques greatly extends our analytical capability when examining LFP materials in terms of structure and chemical information. Due to the high sensitivity of the synchrotron-based techniques, it would be possible to find the subtle change of the chemical composition in LFP, which is very effective at identifying the secondary phases. Therefore, it is expected that these advanced mapping techniques can provide valuable feedback for manufacturing LFP materials and optimizing processes.

REFERENCES

[1]   A. K. Padhi, K. Nanjundaswamy, J. B. Goodenough, *J. Electrochem. Soc.* **1997**, *144*, 1188.

[2]   Y. Wang, P. He, H. Zhou, *Energ. Environ. Sci.* **2011**, *4*, 805.

[3]   L.-X. Yuan, Z.-H. Wang, W.-X. Zhang, X.-L. Hu, J.-T. Chen, Y.-H. Huang, J. B. Goodenough, *Energ. Environ. Sci.* **2011**, *4*, 269.

[4]   J. Wang, X. Sun, *Energ. Environ. Sci.* **2012**, *5*, 5163.

[5]   M. Herstedt, M. Stjerndahl, A. Nytén, T. Gustafsson, H. Rensmo, H. Siegbahn, N. Ravet, M. Armand, J. O. Thomas, K. Edström, *Electrochem. Solid St.* **2003**, *6*, A202.

[6]   N. Ravet, A. Abouimrane, M. Armand, *Nat. Mater.* **2003**, *2,* 702.

[7]   P. S. Herle, B. Ellis, N. Coombs, L. F. Nazar, *Nat. Mater.* **2004**, *3*, 147.

[8]   N. Ravet, Y. Chouinard, J. Magnan, S. Besner, M. Gauthier, M. Armand, *J. Power Sources* **2001**, *97*, 503.

[9]   US. 20040029011 A1, (**2002**), Universite de Montreal, Centre National de la Recherche Scientifique, invs.: N. Ravet, M. Armand.

[10]   J. Wang, J. Yang, Y. Zhang, Y. Li, Tang, Y. M. N. Banis, X. Li, G. Liang, R. Li, X. Sun, *Adv. Func. Mater.* **2013**, *23*, 806.

[11]   J. Wang, J. Yang, Y. Tang, J. Liu, Y. Zhang, X. Li, G. Liang, M. Gauthier, Y.-C. Chen-Wiegart, M. N. Banis, X. Sun, *Nat. Commun.* **2014**, *5*, 3415.

[12]   D. MacNeil, L. Devigne, I. Michot, C. Rodrigues, G. Liang, M.Gauthier, *J. Electrochem. Soc.* **2010**, *157*, A463.

[13]   M. Gauthier, C. Michot, N. Ravet, M. Duchesneau, J. Dufour, G. Liang, J. Wontcheu, L. Gauthier, D. MacNeil, *J. Electrochem. Soc.* **2010**, *157*, A453.

[14]   Y. Liu, J. Liu, J. Wang, M. N. Banis, B. Xiao, A. Lushington, W. Xiao, R. Li, T.-K. Sham, G. Liang, *Nat. Commun.* **2018**, *9*, 929.

Figure Captions

Figure 1. Schematic of LFP and secondary/impurity phases in (a) melt-casting LFP ingot and (b) LFP ingot after carbon coating.

Figure 2. (a) Point Raman spectra of LFP and impurity phase in LFP ingot and (b) optical image.

Figure 3. (a–c) Raman and (d) EDS mapping of different elementals on LFP ingot: impurity phase (low melting phase) identification.

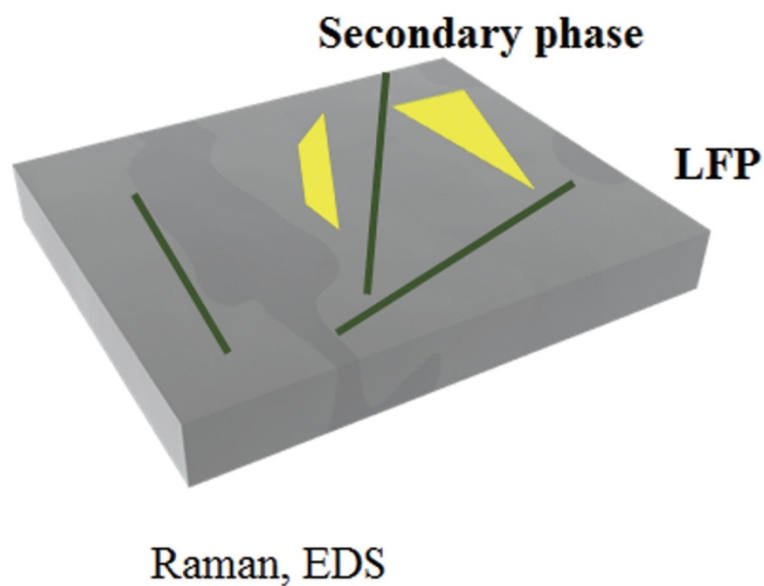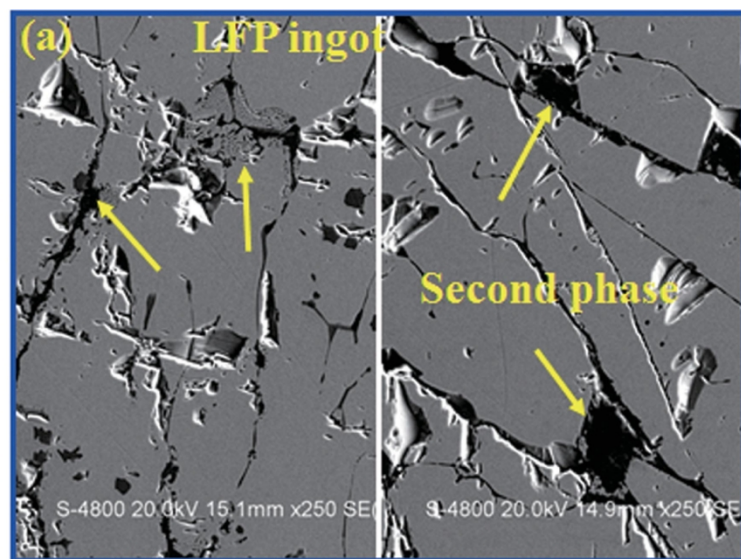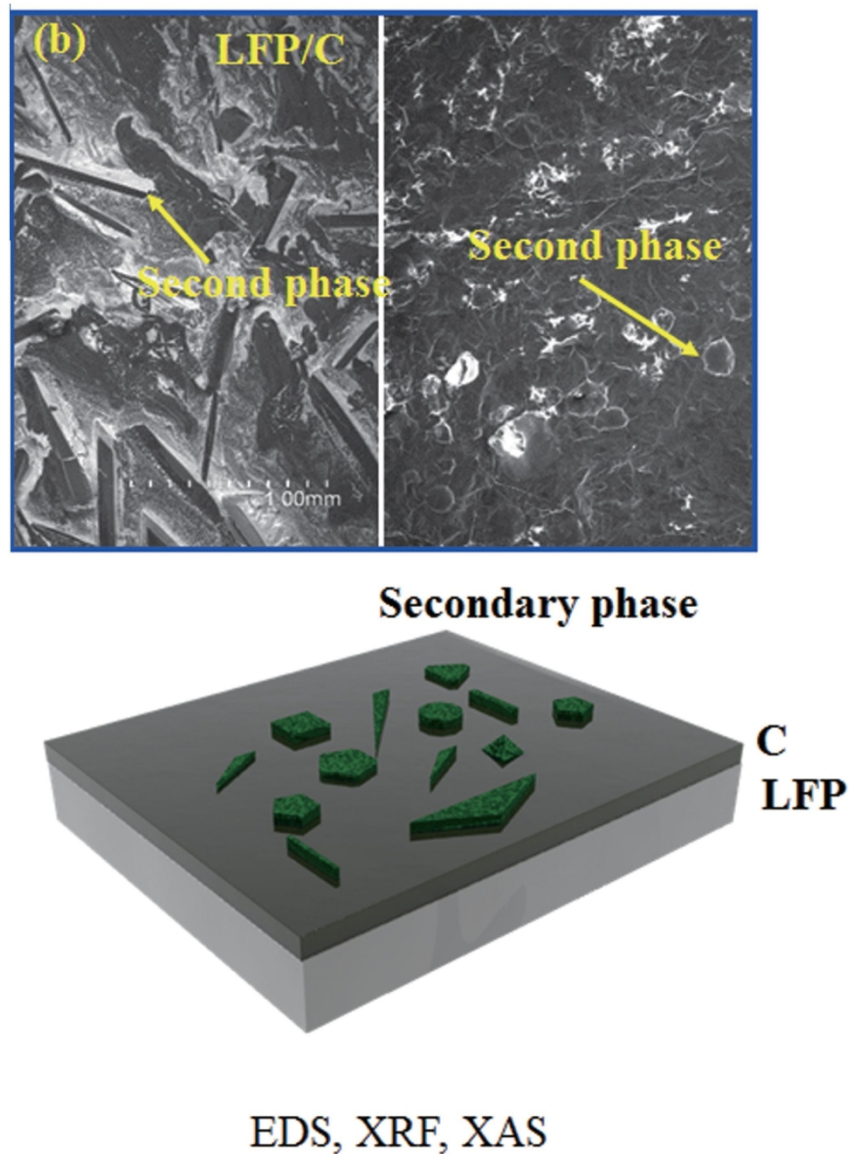Figure 4. (1) Micro XRF mapping and (2) EDS mapping on LFP ingot after carbon coating: phase identification.

Figure 1. Schematic of LFP and secondary/impurity phases in (a) melt-casting LFP ingot and (b) LFP ingot after carbon coating.

118x158mm (300 x 300 DPI)

Figure 1. Schematic of LFP and secondary/impurity phases in (a) melt-casting LFP ingot and (b) LFP ingot after carbon coating.
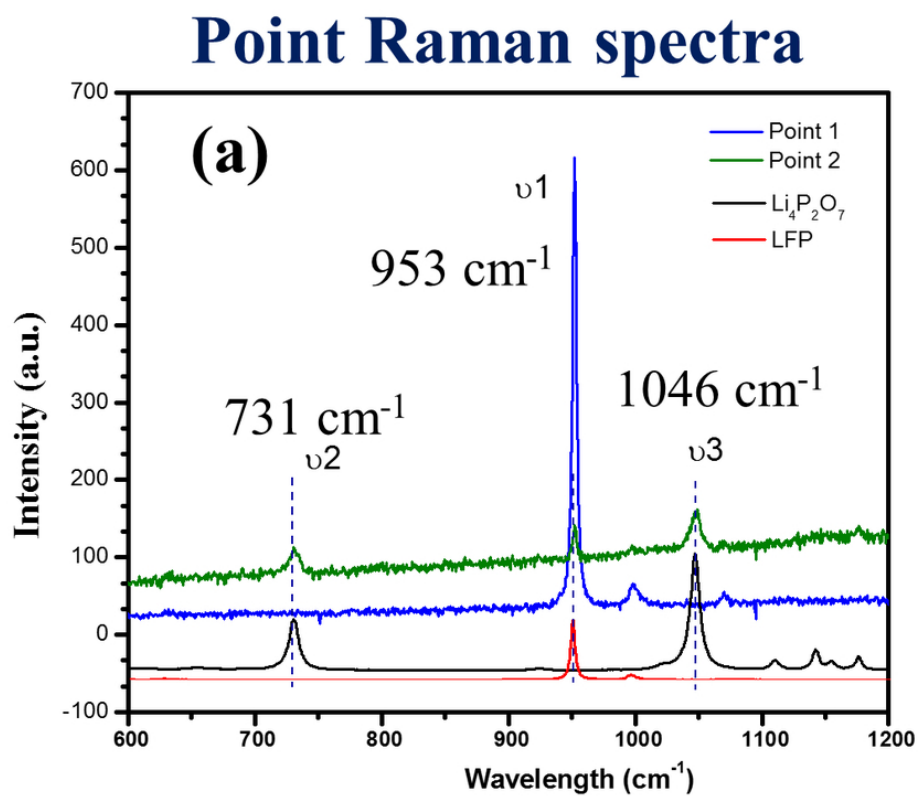
124x175mm (300 x 300 DPI)

Figure 2. Point Raman spectra of LFP and impurity phase in LFP ingot.
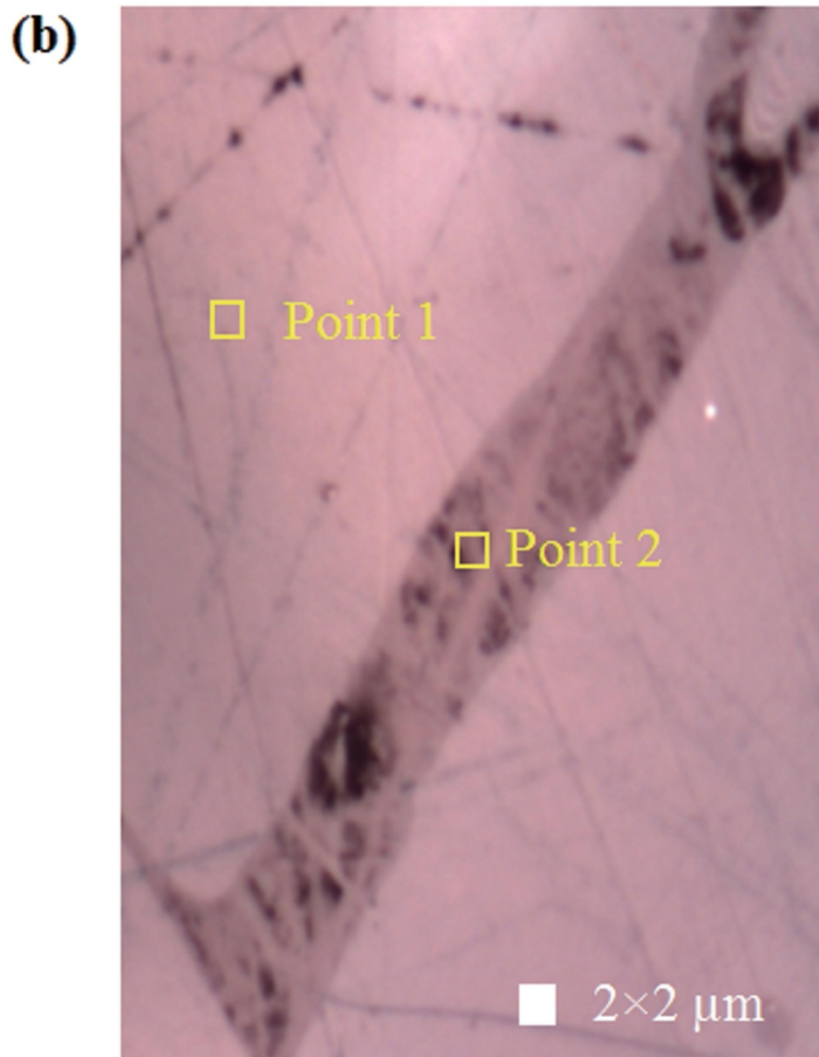
76x66mm (300 x 300 DPI)

Figure 2. Point Raman spectra of LFP and impurity phase in LFP ingot.
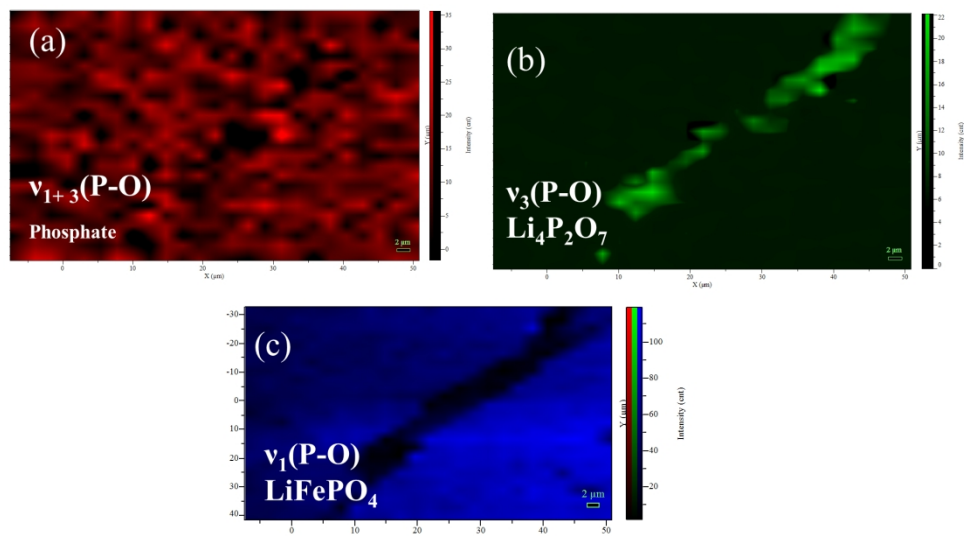
124x175mm (300 x 300 DPI)

Raman mapping

Figure 3. Raman and EDS mapping on LFP ingot: impurity phase (low melting phase) identification.
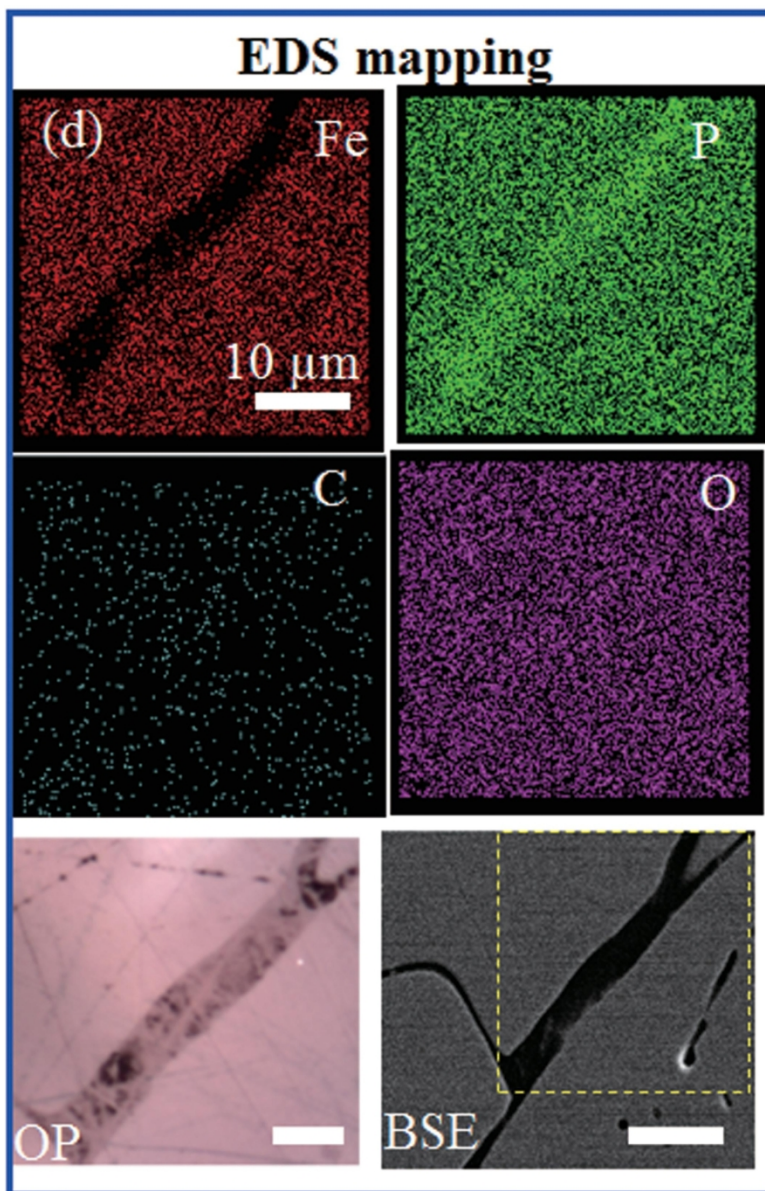
186x122mm (300 x 300 DPI)

Figure 3. Raman and EDS mapping on LFP ingot: impurity phase (low melting phase) identification.
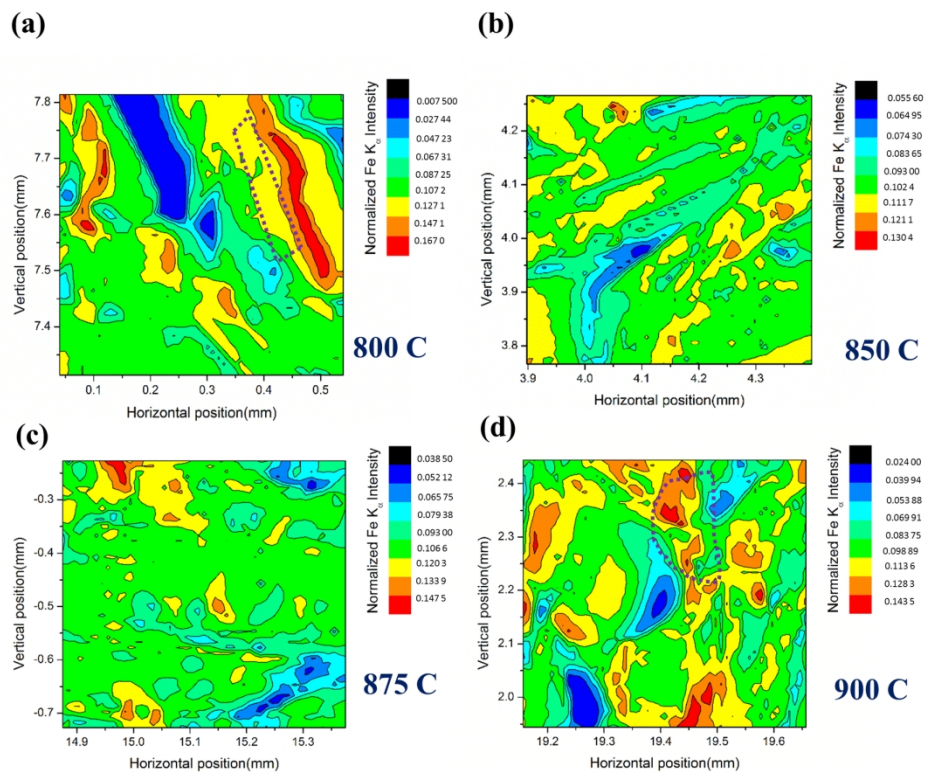
138x214mm (300 x 300 DPI)

Micro XRF mapping

(a)

(b)

(c)

(d)

Figure 4. Micro XRF and EDS mapping on LFP ingot after carbon coating: phase identification.

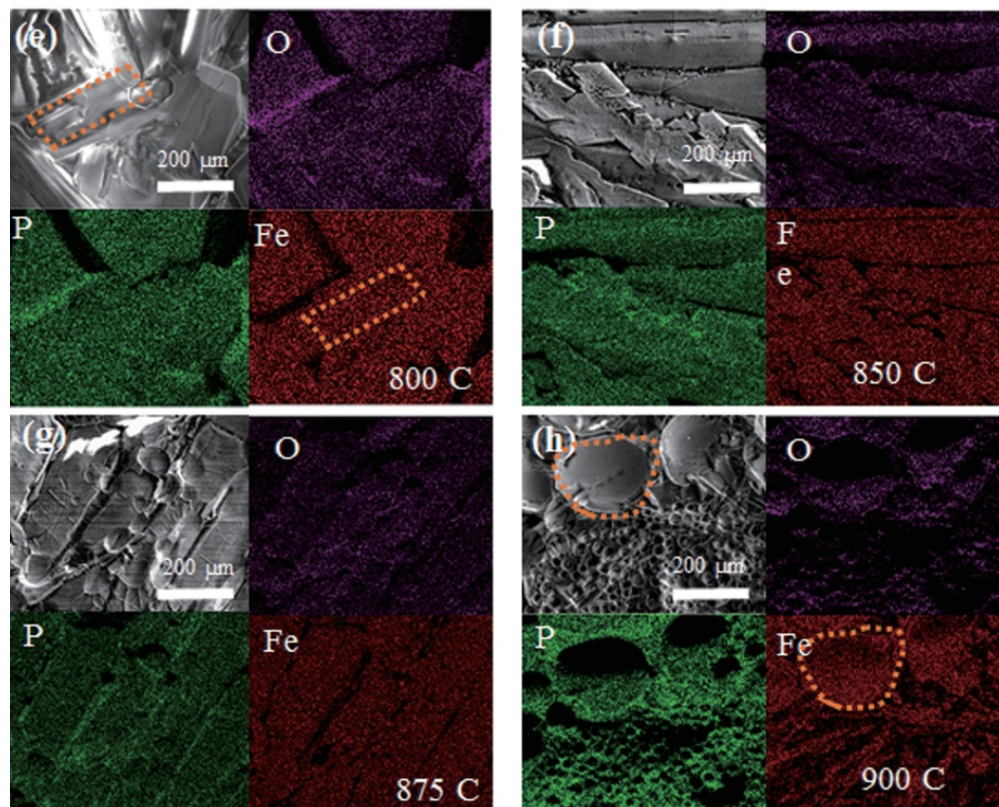161x146mm (300 x 300 DPI)

EDS mapping

Figure 4. Micro XRF and EDS mapping on LFP ingot after carbon coating: phase identification.

80x71mm (300 x 300 DPI)